ChemFoodChem

ChemFoodChem

Chemistry Europe
European Chemical Societies Publishing

RESEARCH ARTICLE OPEN ACCESS

Formation and Characterization of Insoluble Anthocyanins-λ-carrageenan Biopolyelectrolyte Complexes: Structural Morphology, Thermal Stability, and Release Dynamics

Tomás Garrido[1] | Ana Rita Pereira[1,2] | Hiléia K. S. Souza[3] | Nuno Mateus[1,2] | Victor de Freitas[1,2] | Ana Fernandes[2]

[1]Faculdade de Ciências da Universidade do Porto, Porto, Portugal | [2]LAQV/REQUIMTE, Chemistry and Biochemistry Department, Science Faculty, Porto University, Porto, Portugal | [3]CBQF – Centro de Biotecnologia e Química Fina – Laboratório Associado, Universidade Católica Portuguesa, Porto, Portugal

Correspondence: Ana Fernandes (ana.fernandes@fc.up.pt)

Received: 12 January 2026 | **Revised:** 11 March 2026 | **Accepted:** 14 March 2026

Keywords: anionic polysaccharides | blackberry anthocyanin extract | coacervates | hidrogel-like material release rate | thermal stability

ABSTRACT

This study explores the formation of insoluble biopolyelectrolyte complexes based on blackberry anthocyanin (BAE) and λ-carrageenan (λ-CRG). It aims to optimize the conditions that promote complexation between anthocyanin (ANC) molecules and λ-carrageenan, and to understand the physicochemical properties of insoluble BAE-λ-CRG complexes. Blackberry anthocyanin extract was characterized to determine its total phenolic content and anthocyanins, besides its antioxidant potential, with cyanidin-3-*O*-glucoside (cy3glc) being identified as the major anthocyanin present in the extract. Optimal insoluble polyelectrolyte complexe formation conditions were determined at a λ-CRG/BAE weight ratio of 0.05 at pH 3. Physicochemical analyses, including FTIR-ATR, SEM, and thermal stability tests, confirmed successful complexation, with the insoluble complexes exhibiting a porous, hydrogel-like morphology and enhanced thermal resistance. Release studies demonstrated low anthocyanins' release over 8 h, following a Fickian diffusion model, with the diffusional exponent n value being influenced by pH and by the presence of salts. These findings highlight the potential of anthocyanin-carrageenan insoluble complexes as a highly innovative anthocyanin-based material for controlled delivery applications.

1 | Introduction

Anthocyanins are a group of polyphenols categorized within the flavonoid class, naturally occurring in vascular plants [1]. These water-soluble pigments are responsible for plant coloration and display a wide range of colors, from red to purple and blue. Anthocyanins' color depends on factors such as pH, chemical substitutions, copigmentation, and metal interactions, which alter how they absorb and reflect light, thus resulting in different colors [2]. Besides these chromatic features, a myriad of biological activities have been associated with anthocyanins, including antioxidant, anti-inflammatory, or antimicrobial activity. They have also been linked to a reduced risk of neurodegenerative disorders and metabolic syndrome, as well as to prebiotic potential, suggesting a deeper role in human health [3–6]. Consequently, a large interest in incorporating anthocyanin-rich ingredients into the food and healthcare sectors has been generated [7].

However, challenges such as low stability of the extracted compounds to environmental and processing factors, resulting in reduced bioavailability, hinder the utilization of these molecules

as bio- and techno-functional ingredients [8, 9]. Consequently, new approaches to enhance the stability of anthocyanins, improve their biological potential, while providing selective or controlled release, have been searched. At the same time, there is a clear need to identify appropriate matrices that fulfill the diverse requirements specified for anthocyanins industrial implementation. Biopolymers such as polysaccharides have been shown to be versatile matrices in the food and health sectors [10], allowing the production of polysaccharide-based films, hydrogels, nanoparticles, or microparticles. Among these, biopolyelectrolyte complexes (bioPECs), which are formed when oppositely charged polymers (polyelectrolytes) interact through ionic interactions [11], present an attractive possibility to overcome the limitations of anthocyanins and promote their targeted delivery [12–15]. The production of bioPECs does not require high energy, chemical crosslinkers, or organic solvents [16]. However, factors like pH, salt concentration, charge distribution, mixing conditions, and molecular weight can affect bioPECs morphology and yield. BioPECs formation generally involves three steps: initial molecule interaction to form the primary complex, intermediate complex formation via electrostatic bonds, creating a polymeric chain, and aggregation through hydrophobic interactions [11, 17]. At stoichiometric charge ratios (close to charge neutrality), insoluble complexes (or coacervates) and generated by liquid–liquid phase separation of the molecular components of a solution [18, 19]. On the other hand, soluble complexes may be formed if excess charges, or when weak interactions are present.

Interestingly, bioPEC-like complexes, which can be referred to as structures that are formed when small and charged molecules (like anthocyanins) interact with one polyelectrolyte, have also been shown to provide a protective microenvironment for anthocyanins [20–22]. This interaction can be achieved through the electrostatic interaction of anthocyanins' flavylium cation with negatively charged biopolymers, with hydrogen bonding and hydrophobic interactions also occurring. Dextran sulfate was used to create PEC-like complexes by combining it with bilberry extract [23]. The negatively charged sulfate groups present in this polysaccharide stabilized the bilberry extract, due to the formation of electrostatic interactions with anthocyanins' flavylium cation. However, it was shown that different total concentrations and weight ratios affected the formation of both soluble and insoluble complexes. Chondroitin sulfate, was also used to form PEC-like complexes with black soybean anthocyanins [24]. The results showed the formation of soluble nanocomplexes, resulting from π-π interactions between anthocyanin moieties, and ionic interactions between sulfate groups and the positively charged molecules from the 2-phenylbenzopyrylium backbone of anthocyanins. Carrageenan, a mucopolysaccharide, was also tested as a counterion to form bioPEC-like complexes. This sulfated polygalactan is naturally present in different seaweed species such as *Chondrus crispus*, or *Kappaphycus alverezii* [25]. ι- and κ-carrageenan, with two and one sulfate group, respectively, were used to form bioPEC-like complexes with blueberry anthocyanins [16].

Although bioPEC-like complexes have been extensively investigated to improve anthocyanins' stability, research has predominantly focused on soluble particles, while anthocyanins-based insoluble complexes remained largely unexplored. However, insoluble complexes may present significant advantages, including enhanced stability of anthocyanins against degradation (e.g., temperature, pH), the potential for controlled release under specific environmental or physiological conditions, and the ability to function as innovative ingredients in applications such as active food packaging, biomedical materials, and pH-responsive colorimetric sensors, as they may display unique properties. Therefore, the systematic investigation of the formation mechanisms, physicochemical properties, and functional performance of insoluble anthocyanin–bioPECs is essential to elucidate their full technological potential and expand their technological applicability.

2 | Materials and Methods

2.1 | Materials

Analytical grade reagents were used in the study. 2,4,6-Tris(2-pyridyl)-s-triazine (TPTZ), acetic acid, formic acid, acetonitrile, methanol, and sodium hydroxide were acquired from Chem-Lab (USA), while C18 silica gel was obtained from Fluka. 2,2-diphenyl-1-picrylhydrazyl (DPPH), 2-(N-morpholino)-ethanesulfonic acid (MES), Bradford reagent, citric acid monohydrate, ethyl acetate, Folin-Ciocalteu reagent, λ-carrageenan (λ-ARG), sodium acetate trihydrate, sodium phosphate dibasic dihydrate, and trolox were obtained from Sigma Aldrich, St. Louis, MO, USA. Honeywell (USA) supplied hydrochloric acid, while Panreac AppliChem provided phosphate saline buffer tablets (PBS) and sodium carbonate. Ultrapure water, produced by a MilliQ filtration system, was used for the preparation of all solutions.

2.2 | Anthocyanins Extraction and Purification

Frozen blackberries were macerated with acidified (2% HCl) deionized water (1:10 *w/v*). The mixture was stirred for 4 h at room temperature and after this period, the residues were filtered on a porous tissue and subjected to a second water extraction for 20 h at room temperature (24 h total extraction time). The crude extract was centrifuged at 10,000 rpm for 10 min at 20°C (Dynamica Velocity 14R Refrigerated Centrifuge, Dynamica Scientific Ltd.; Livingston, United Kingdom), and the supernatant was purified using reverse-phase C18 silica gel, with acidified deionized water to remove simple sugars, salts, and organic acids. The anthocyanic fraction was then recovered with acidified methanol, and the solvent was evaporated under vacuum at 37°C. The resulting blackberry anthocyanin-rich extract (BAE) was diluted in ultrapure water, freeze-dried, and stored at -20°C until further use.

2.2.1 | Total Phenolic Content

The total phenolic content (TPC) of BAE was determined using the Folin-Ciocalteau method [26]. 15 µL of the blackberry anthocyanin extract (1 mg/mL) was added to a microtube, followed by the addition of 75 µL of Folin-Ciocalteau reagent. Then, 1110 µL of ultrapure water was added, and the microtube was thoroughly mixed. 300 µL of 5% Na_2CO_3 were added and mixed again. The samples were left to stabilize for 30 min in the dark.

Blank samples were prepared with ultrapure water. All samples were prepared in triplicate. For the measurement, 350 µL of the samples and blanks were pipetted into a 96-well plate, and the absorbance was measured at 750 nm using a plate reader (Biotek Powerwave XS, Santa Clara, CA, USA). The total phenolic content was expressed as µg gallic acid equivalents (GAE)/mg of BAE.

2.2.2 | Low Molecular Weight Phenolic Compounds Quantification by HPLC-DAD

The quantification of low molecular weight phenolic compounds in BAE was carried out using High Performance Liquid Chromatography coupled with Diode Array Detector (HPLC-DAD). Firstly, BAE (1.0 mg/mL) was subjected to a liquid-liquid extraction with an ethyl acetate/acetonitrile mixture (2/2/1 *v/v/v*) to isolate the low molecular weight phenolic compounds. The resulting organic phase was recovered, and the aqueous phase was extracted again using the same procedure. The organic fractions were combined, dried, and resuspended in a MeOH/H_2O (50/50) mixture. The HPLC-DAD analysis (20 µL injection volume) was performed using a reverse phase column from Merck (LiChrospher 100, LiChroCART, 150×4 mm inner diameter; 5 µm particle size) at 25°C, with a flow rate of 0.3 mL/min. The solvents used were H_2O/CH_3COOH (solvent A, 99/1 *v/v*) and H_2O/CH_3COOH/CH_3CN (solvent B, 79/1/20 *v/v/v*). The elution gradient was used as follows: 0 min to 55 min, 80% of solvent A to 20% of solvent A; 55 min to 70 min, 20% of solvent A to 10% of solvent A; 70 min to 80 min, 10% of solvent A to 0% of solvent A; 80 min to 90 min, 0% of solvent A to 80% of solvent A. For the estimation of the overall content of low-molecular weight phenolic compounds, results were expressed as µg GAE/mgof BAE, using a calibration curve made with gallic acid as a reference compound.

2.2.3 | Anthocyanin Quantification and Identification by HPLC-DAD and HPLC-DAD/ESI-MS

The anthocyanin content in BAE was measured using HPLC-DAD. 20 µL of the extract (1.0 mg/mL) was injected into a reversed phase C18 column from Merck (LiChrospher 100, LiChroCART, 250×4 mm inner diameter; 5 µm particle size) at 25°C. The detection was carried out in the wavelength range of 200 nm to 700 nm. Mass detection was performed using a Finnigan LCQ DECA XP MAX mass detector, operated at a flow rate of 0.5 mL/min, with atmospheric pressure ionization and an electrospray ionization interface. The capillary voltage was set at 4 V, with a capillary temperature of 325°C. Mass spectra were acquired in positive ion mode, with a mass-to-charge ratio (*m/z*) range of 0 to 2000. Three scans were conducted: a full-mass scan, a zoom scan on the most intense ion, and a MS-MS scan of the ion using collision energy of 30 V and 60 V.

For HPLC-DAD analysis, the mobile phases used consisted of a mixture of H_2O/HCOOH (90/10 *v/v*) (Solvent A) and a mixture of H_2O/HCOOH/CH_3CN (60/10/30 *v/v/v*) at a flow rate of 1.0 mL/min. The elution gradient was as follows: 0 min to 70 min, 80% to 15% of solvent A; 70 min to 75 min, 15% to 0% of solvent A; 75 min to 85 min, 0% of solvent A; and 85 min to 95 min, 0% to 80% of solvent A. Results were expressed as µg cyanidin-3-*O*-glucoside (cy3glc) equivalents/mg of BAE. Anthocyanins identification was carried out using HPLC-DAD/ESI-MS with the same elution gradient at a flow rate of 0.4 mL/min, using a mixture of H_2O/HCOOH (99/1 *v/v*) (solvent A) and a mixture of H_2O/HCOOH/CH_3CN (69:1:30) (solvent B) as mobile phases.

2.2.4 | Protein Quantification

The Bradford method was used to determine the soluble protein content in BAE [27]. 100 µL of the extract (0.5 mg/mL) or ultrapure water was mixed with 200 µL of Bradford's reagent. The mixture was allowed to stabilize in the dark at room temperature for 10 min, and the absorbance was read at 595 nm using a plate reader (Biotek Powerwave XS, Santa Clara, CA, USA). The protein content was expressed as µg bovine albumin serum equivalents/mg of BAE.

2.2.5 | Antiradical Activity

The antiradical activity of the BAE was assessed using the DPPH (2,2-diphenyl-1-picrylhydrazyl) radical assay. Three solutions were prepared, including a blank sample with ultrapure water and the BAE, a control sample with DPPH and ultrapure water, and a sample with DPPH and the BAE (1 mg/mL). The DPPH solution was prepared at 60 µM in methanol. All solutions were prepared in quadruplicate. Absorbance readings were taken at 515 nm using a plate reader (Biotek Powerwave XS, Santa Clara, CA, USA) at 0 min, 5 min, 10 min, 15 min, and 20 min. The results were expressed as µM equivalents of Trolox, after 20 min reaction.

2.2.6 | Ferric Reducing Capacity

The BAE ferric reducing capacity was assessed by measuring the reduction of $[Fe(III)\text{-}TPTZ_2]^{3+}$ to $[Fe(II)\text{-}TPTZ_2]^{2+}$ at pH 3.6, in the presence of antioxidants. The Ferric Reducing Antioxidant Power (FRAP) reagent was prepared by combining a 300 mM acetate buffer solution (pH 3.6) with 10 mM TPTZ (prepared in 40 mM HCl) and 20 mM $FeCl_3$. The resulting mixture was diluted by one-third with acetate buffer and incubated at 37°C for 15 min. The samples were prepared in ultrapure water at a concentration of 0.1 mg/mL, with the control consisting of FRAP reagent and ultrapure water, and the blank consisting of ultrapure water and the sample. Each solution was prepared in quadruplicate, and the absorbance was measured at 593 nm using a plate reader (Biotek Powerwave XS, Santa Clara, CA, USA) at 0 min and 4 min, at 37°C. The results were expressed in terms of µM equivalents of Trolox.

2.3 | Blackberry Anthocyanins and λ-carrageenan Complexes

2.3.1 | Solutions Preparation

λ-CRG (0.1% *w/w*) was dissolved in 10 mM acetate buffer (pH 2.5, 3.0, and 4.0) and heated at 80°C for 10 min until complete dissolution. The solutions were cooled to room temperature, and the pH was adjusted, if needed. Similarly, BAE solutions (0.1%

w/w) were prepared in acetate buffer at room temperature. Before use, solutions were centrifuged at 13,000 rpm for 2 min to remove any residual insoluble impurities, then allowed to equilibrate for at least 1 h.

2.4 | Interaction Conditions: Determination of the Optimal Ratio

2.4.1 | Optical Dispersion Measurements

Optical dispersion measurements were conducted to determine the optimum conditions for insoluble complex formation, based on Tavares et al., [28]. Aliquots of λ-CRG solution were gradually added to 750 μL of BAE in the UV-Vis cell and homogeneized. The optical dispersion of these solutions was measured at 650 nm using an Evolution Array UV-Visible Spectrophotometer from Thermo Scientific. The assays were performed at pH 2.5, 3.0, and 4.0, in acetate buffer (10 mM). The impact of λ-CRG/BAE ratio (% weight (*w/w*)) on the solution optical dispersion was determined in triplicate.

2.4.2 | Zeta Potential Measurements

To determine the charge balance in the formation of insoluble complexes, λ-CRG and BAE solutions were prepared as previously described and filtered (0.45 μm syringe filters). Mixtures of λ-CRG and BAE were prepared at the optimum interaction ratio (determined in *section 2.4.1*), mixed continuously for 2 h, and centrifuged at 12,500 rpm at 20°C for 10 min. The superficial charge values (ζ-potential) were measured through electrophoretic light scattering (ELS) with a Malvern Zetasizer Nano ZS instrument from Malvern Instruments Ltd., UK. All assays were performed in triplicate, using water as a dispersant agent at 25°C, and data were presented as mean ± standard deviation (SD) in millivolts (mV).

2.4.3 | Incorporation Rate and Loading Capacity of λ-CRG

The amount of anthocyanins incorporated into the BAE-λ-CRG insoluble complexes at the optimum interaction conditions was determined and expressed as the incorporation rate and loading capacity of λ-ARG, according to Klimaviciute et al., [23]. For the control sample, BAE was prepared at the same concentration as for the complex. The concentration of anthocyanins in the supernatant was determined by HPLC-DAD, according to the method as described in *section 2.2.6*. The results were expressed as the incorporation rate and loading capacity, calculated using the following equations:

$$Incorporation\ rate = \left(\frac{(cy3glc)_{control} - (cy3glc)_{sample}}{(cy3glc)_{control}} \right) \quad (1)$$

$$Loading\ capacity = \left(\frac{(cy3glc)_{contral} - (cy3glc)_{sample}}{(\lambda{-}CRG)} \right) \quad (2)$$

2.5 | Optimized Preparation of Insoluble Complexes

For the preparation of BAE-λ-CRG insoluble complexes, a BAE 0.1% (*w/w*) solution was added to λ-CRG 0.1% (*w/w*) solution according to the optimum λ-CRG/BAE ratio determined by turbidity measurements. The mixture was stirred for 2 h at 120 rpm. Thereafter, the two formed phases were separated through centrifugation (10 min at 12,500 rpm). The pellet (BAE-λ-CRG insoluble complexes) was recovered, washed twice with ultrapure water to remove any unbound anthocyanins, and freeze-dried for further physicochemical characterization.

2.6 | Physicochemical Characterization of BAE-λ-CRG Insoluble Complexes

2.6.1 | Scanning Electron Microscopy (SEM) and Cryo-scanning Electron Microscopy (Cryo-SEM)

The observation and analysis of the microstructure of dried BAE, λ-CRG, and the insoluble BAE-λ-CRG complexes were performed by scanning electron microscopy (SEM) with a FEI Quanta 400 FEG ESEM/EDAX Genesis X4M device. The samples were positioned on aluminum supports and coated with a thin layer of Au-Pd to enhance electron conductivity. The SEM images were obtained using an acceleration voltage of 15 kV, a working distance of 10 mm, and a magnification level ranging from 500x to 15000x.

The microstructure of wet BAE-λ-CRG complexes (before freeze-drying) was also analyzed by scanning electron cryo-microscopy (cryo-SEM). A JEOL JSM 6301F Oxford INCA Energy 350 electron microscope, equipped with a Gatan Alto 2500 cryo-preparation chamber, was used for this purpose. The complexes were frozen in liquid nitrogen at -200°C and then fractured. Solvent sublimation was carried out at -90°C for 120 s, and an Au-Pd layer was coated onto the sample using a SPI Module Sputter Coater. The microscopic image was obtained at -150°C with an acceleration voltage of 15 kV, a working distance of 15 mm, and a magnification level of 5000x to 10000x.

2.6.2 | Ftir-Atr

FTIR-ATR data were obtained for BAE-λ-CRG insoluble complexes, λ-CRG, and BAE at room temperature using PerkinElmer Spectrum Two (USA) equipment. For each sample, around 1 mg of the material was placed on a crystal made from synthetic diamond, and spectra were collected in the range of 4000 cm^{-1} to 400 cm^{-1}.

2.6.3 | Thermal Stability

The thermal stability of the BAE-λ-CRG complexes was evaluated using simultaneous thermal analysis (STA), which combines dynamic scanning calorimetry (DSC) and thermogravimetry (TGA). The STA experiment was performed at a heating rate of 5°C/min using a Hitachi Instruments STA7200RV from Hitachi Instruments, Inc. (Japan). Approximately 10 mg of each sample

was placed in an open aluminum crucible, and the measurements were carried out between 20°C and 400°C under an inert atmosphere. The thermal stability of BAE-λ-CRG complexes was compared to that of BAE and λ-CRG, analyzed using the same methodology.

2.6.4 | Release Studies: Anthocyanins Desorption From BAE-λ-CRG Complexes

The anthocyanins release pattern from BAE-λ-CRG insoluble complexes was studied at 3 pH values. Uniform powdered BAE-λ-CRG insoluble particles were incubated at 5.0 mg/mL in ultrapure water at pH 1.7, 5.4, and 7.4, and in MES buffer at 10 mM (pH = 5.4) or PBS buffer at 10 mM (pH = 7.4) [29]. To prepare ultrapure water at different pH values, HCl (6 M) or NaOH (1 M) was used to adjust pH. Assays were performed for 8 h, under agitation at room temperature, using an Advanced Vortex Mixer ZX3 from VELP Scientifica. Aliquots of 60 μL were collected periodically, and the same volume of each solution was replaced. Aliquots were acidified with 12 μL of HCl 6 M and allowed to equilibrate at room temperature overnight, guaranteeing the total conversion to flavylium cation equilibrium form. Anthocyanins release was evaluated by HPLC-DAD, according to the methodology described in *section 2.2.6*. Release profiles were fitted to the Korsmeyer-Peppas model, according to equations 3 and 4:

$$M_t / M_x = Kt^n \quad (3)$$

$$\log(M_t/M_x) = n\log(t) + \log(K) \quad (4)$$

where, M_t, M_x, K, and n refer to the amount of anthocyanins released in time t, the overall mass of releasable anthocyanins present in the sample, the release rate constant, and the diffusional exponent, respectively. The Korsmeyer–Peppas model is valid for the first 60% of the fractional release and useful to describe various mechanisms of transport, including Fickian diffusion and non-Fickian transport [30]. By employing this approach, the slope of the curves was derived using linear logarithmic equations, and the coefficient of determination (R^2) was calculated. Release studies were performed in triplicate.

2.7 | Statistical Analysis

The results were presented as mean ± standard deviation (SD) and were statistically analyzed using one-way ANOVA followed by the Tukey's test of multiple comparisons to compare means between different samples. The statistical analysis was performed using Prism 9.1.1 (GraphPad software) for MacOS.

3 | Results and discussion

In this work, the formation and characterization of insoluble complexes based on the polyelectrolyte interaction between an anthocyanin-rich extract and an anionic polysaccharide (λ-CRG) was explored. λ-CRG, which contains three sulfate groups, was selected as it is expected to interact more strongly with anthocyanins' flavylium cations, thereby enhancing the stabilization of the anthocyanin extract.

3.1 | Blackberry Anthocyanin Extract Characterization

HPLC-DAD analysis was employed to characterize the extract obtained from blackberries (Table 1). BAE exhibited a high concentration of total phenolic compounds (TPC) (390±37 μg gallic acid equivalents/mg dried BAE), determined using the Folin-Ciocalteu assay, and a relatively low protein content of 65±11 μg BSA/mg dried BAE. The HPLC-DAD analysis showed that BAE was an anthocyanin-rich extract, accounting for roughly 557±65 μg of cy3glc equivalents/mg dried BAE, while the low molecular weight phenolic compounds represented about 73±14 μg of GAE/mg dried extract. The chromatographic profile at 520 nm showed the presence of four significant peaks, corresponding to cyanidin-derivatives, namely, cyanidin-3-*O*-glucoside ($[M+H]^+$ 449/MS^2 287), which was the most abundant anthocyanin with approximately 92% of the total anthocyanin amount quantified in the extract, followed by cyanidin-3-*O*-xylose ($[M+H]^+$ 419/MS^2 287) (4%), cyanidin-3-*O*-(6"-malonyl-glucoside) ($[M+H]^+$ 535/MS^2 287) (2%), and cyanidin-3-*O*-dioxalyl-glucoside ($[M+H]^+$ 593/MS^2 287) (2%). The identification of these peaks was accomplished through HPLC-DAD/ESI-MS analysis and cross-referenced with previously published studies on blackberry extracts [31, 32].

A slightly higher value of anthocyanin content (661 μg.mg^{-1}) could be observed in a study performed by Chen et al., 2023 [33]. However, both studies could demonstrate the efficiency of implementing purification and concentration steps in enriching the extract in the targeted compounds, compared to simple extraction procedures. Additionally, this improvement also shows that purification steps could enhance the selectivity and stability of anthocyanins in the final extract, which may also enhance the production of insoluble complexes. The high anthocyanin content in the extract may have contributed to its ability to sequester free radicals (20±1 μM Trolox equivalents) and strong reducing power (196±18 μM Trolox equivalents).

3.2 | pH Optimal Values in the Formation of BAE-λ-CRG Insoluble Complexes

To determine the maximum interaction between BAE and λ-CRG directly affecting the formation of insoluble aggregates, a spectrophotometry assay was performed. The optical dispersion of the solutions was measured at various λ-CRG-to-BAE ratios, and Figure 1 shows the effect of increasing λ-CRG (0.1%) concentration on the optical dispersion (OD) at 650 nm, using a 0. 1% BAE stock solution. As BAE-λ-CRG interactions are strongly dependent on pH, the working pH range for this study was chosen based on the likelihood of electrostatic interactions occurring in the system. At acidic pH levels (pH<2), anthocyanins exhibit positive charges due to the presence of the flavylium cation form [34]. With pH increase (pH 2–4), the flavylium cation undergoes immediate proton transfer reactions leading to the neutral quinoidal bases. Additionally, the flavylium cation starts

TABLE 1 | Characterization of the blackberry-anthocyanin rich extract.

TPC	LWP	ANCs	PC	DPPH	FRAP
(μg GAE/mg of extract)	(μg eq. GAE/mg of extract)	(μg cy3glc/mg of extract)	(μg eq. BSA/mg of extract)	(μM Trolox equivalents)	(μM Trolox equivalents)
390 ± 37	73 ± 14	557 ± 65	65 ± 11	20 ± 1	195 ± 18

Abbreviations: ANCs, anthocyanins; DPPH, antiradical activity; FRAP, ferric reducing capacity; LWP, low weight phenolic compounds; PC, protein content; TPC, total phenolic content.

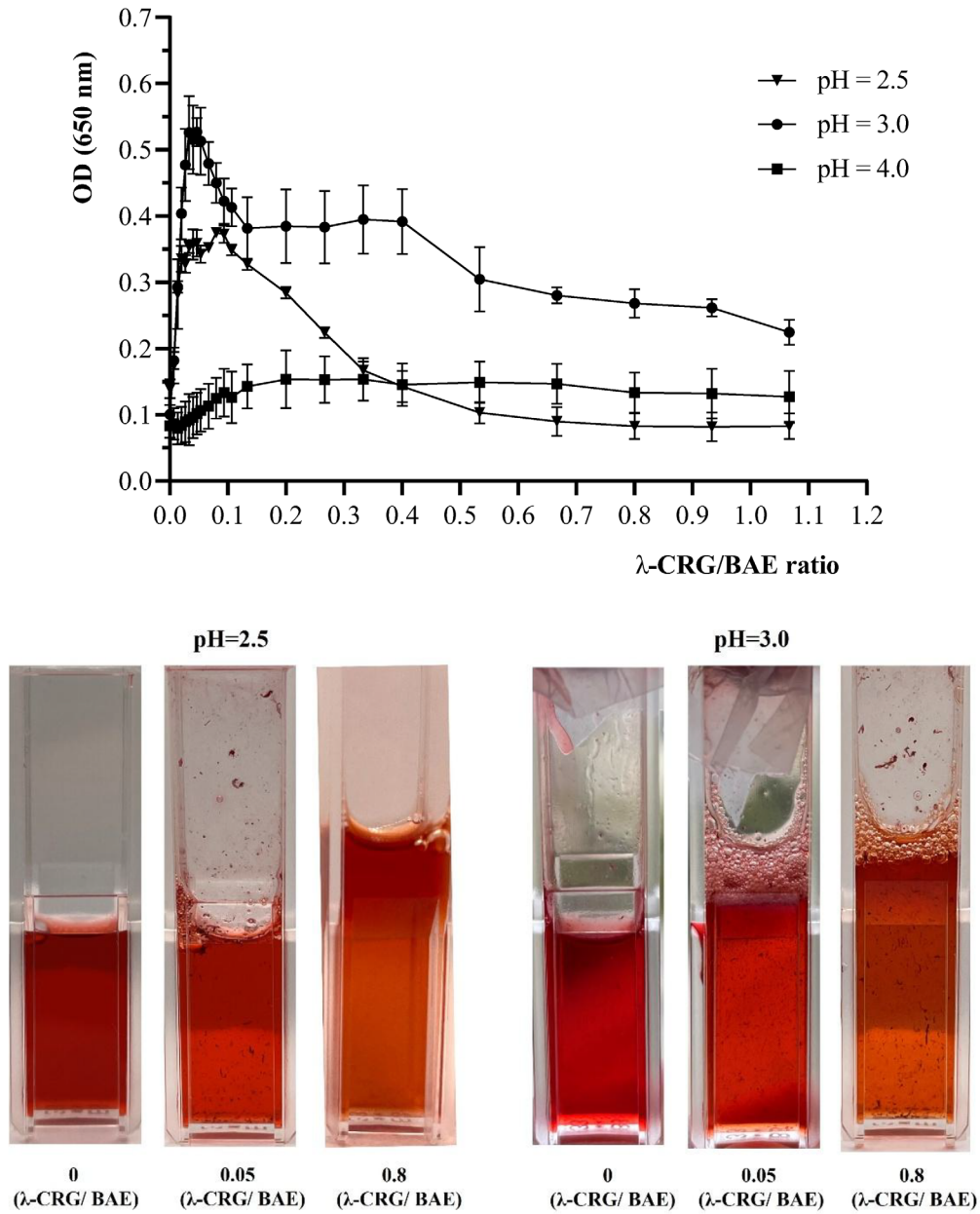

FIGURE 1 | Influence of BAE/λ-CRG mass ratio (% weight w/w), on the OD of BAE 0.1% (w/w) solutions with aliquots of λ-CRG 0.1% (w/w) solutions at pH 2.5, 3.0, and 4.0. Results are presented as mean ± standard deviation. On the bottom, pictures of each interacting system at different weight ratios for pH 2.5 and 3.0).

to hydrate, giving rise to the neutral hemiketal form, which rapidly suffers tautomerization to give the *cis*-chalcone, which further isomerize to the *trans*-chalcone. At higher pH values, further deprotonation occur, turning the solutions blue-green due to the predominance of the quinoidal anionic bases. Meanwhile, λ-CRG remains negatively charged across all pH levels due to the presence of sulfate groups within the polygalactan structure [35]. Therefore, the working pH range was set at 2.5-4.0, which should promote electrostatic interactions between negative sulphate groups of λ-CRG, and the positively charged anthocyanin molecules.

During the titration experiments, the formation of insoluble solid precipitates was shown to be dependent on the pH of the medium and on the weight ratio of anthocyanins and λ-CRG. As shown in Figure 1, at pH 2.5, the addition of increasing volumes of λ-CRG to a BAE solution led to a progressive optical dispersion increase until reaching the point of maximum interaction at an OD around 0.375 and a λ-CRG/BAE weight ratio around 0.08-0.1. At the maximum interaction, the oppositely charged molecules become mutually neutralized and stoichiometrically equal, leading to the formation of insoluble complexes, which could aggregate into large particles and be responsible for the increase on the optical dispersion of the solutions. Beyond this weight ratio, the optical dispersion began to gradually decrease when BAE molecules became saturated with λ-CRG and the charge balance drifted away from the stochiometric charge ratio [28]. Indeed, as more λ-CRG was added to the solution, excess negatively charged sulfate groups remained unbound, potentially leading to an increased solubility of the formed complexes, which might have become soluble and contributed to the significant reduction of the solution optical dispersion (OD similar to the value obtained at the beginning of the titration) [36]. Interestingly, a rapid color change in the samples was observed, shifting from red (in the absence of λ-CRG) to orange at the point of maximum interaction, indicating a hypsochromic shift. This color change has been previously reported in studies examining the interaction between anthocyanins and anionic polysaccharides, such as dextran sulfate, attributed to the occurrence of electrostatic interactions [23]. Conversely, Jeon et al., [24] reported that the complexes formation between chondroitin sulfate and anthocyanins led to a bathochromic shift. In that study, complex formation was influenced not only by electrostatic interactions between sulfated groups in polysaccharides but also by hydrophobic interactions and anthocyanins' intermolecular stacking.

At pH 3, a sharp increase in the optical dispersion of the solution was observed at a lower λ-CRG/BAE weight ratio, showing a maximum interaction at a weight ratio of 0.03-0.05 and reaching an OD around 0.526, markedly higher than that recorded at pH 2.5. After this weight ratio, a decrease in the optical dispersion of the solution was observed, followed by stabilization in the OD values between 0.13 and 0.4 λ-CRG/BAE weight ratios. A new plateau was then reached at the λ-CRG/BAE weight ratio of 0.5, after a slight decrease in the OD value. The moderate decrease in the optical dispersion of the solution could be attributed to the higher stability of the formed complexes at this pH value, which were able to resist when more λ-CRG was added to the BAE solution [28]. In fact, at the end of the titration, at the weight ratio of 0.8, it was still possible to presence of insoluble complexes, on the opposite to what was observed at pH 2.5. Color changes from red to orange were also observed, possibly indicating electrostatic interactions taking place.

TABLE 2 | Values of ζ-potential (mV) expressed as mean ± SD. For each row, samples with the same symbol (*) do not present statistical differences ($p>0.05$).

	pH 2.5	pH 3.0	pH 4.0
BAE	25.7 ± 0.6	12.5 ± 0.2	-15.4 ± 0.9
λ-CRG	-33.0 ± 0.5	-43 ± 2*	-42.3 ± 0.8*
BAE/λ-CRG	12.7 ± 0.5	-3.4 ± 0.4	-38.8 ± 0.9

At pH 4, a slight increase in optical dispersion was observed, but no noticeable formation of insoluble complexes occurred. At this pH value, the flavylium cation is in thermodynamic equilibrium with the hemiketal form and quinoidal base, which reduces the availability of flavylium cation for electrostatic interactions with λ-CRG.

Based on the results above, the measured optical density provided insights into the formation of insoluble complexes at three different pH levels. The choice of pH plays a critical role in determining the outcome of complex formation, as pH variations significantly affect the net charge of the solid complexes. Changes in pH can lead to a decrease in the stoichiometric ratio of negative to positive charges, which, in turn, can cause conformational changes in the polymer network of the complexes [11]. To further investigate the net charge formed during the complexation reaction, the superficial charge of individual compounds and complexes was measured by DLS. For this assay, stock solutions of BAE, λ-CRG, and the BAE-λ-CRG complexes at a weight ratio of 0.05 (λ-CRG/BAE) were prepared as previously described, and the superficial charges (ζ-potential) of the resulting supernatant, as well as the stock BAE and λ-CRG solutions, were measured. The data is shown in Table 2.

The superficial charge of BAE samples at different pH values was significantly different ($p<0.05$). ζ-potential value showed a decrease on the superficial charge from pH 2.5 to 4.0 (from 25.7 to -15.4), due to the changes on ANCs chemical equilibrium forms present in solution, including the flavylium cation form and the neutral hemiketal and quinoidal bases. Furthermore, acetate buffer at pH 4 may also contribute to a more negatively charged environment observed, contributing to the decrease that was observed [37].

For λ-CRG, the superficial charge was negative for all measured pHs, although less negative at pH 2.5 ($p<0.05$), in accordance with the values described in the literature [38]. For the supernatant resulting from the BAE-λ-CRG interaction, significant differences were observed in the ζ-potential value ($p<0.05$) when compared to the BAE and λ-CRG solutions. A positive value was recorded at the lowest pH value, becoming almost neutral at pH 3.0 (-3.4 mV) and negative at pH 4.0. When ζ-potential is close to zero, as in the case of pH 3.0, the precipitation of insoluble complexes from the liquid phase occurs due to charge neutralization between charged moieties. Additionally, if ζ-potential value drifts away from 0, electrostatic interaction in the complex may become weaker, thus affecting the physical properties of the complexes

[39]. In a previous work, complex coacervates made by the interaction of gum arabic and chitosan were studied regarding their viscoelastic properties obtained by changing the ratio of the two biopolymers [39] ζ-potential value showed a deviation from neutrality as the ratio of gum arabic:chitosan changed from 3:1 to 5.5:1, showing a decrease in the yield of coacervates and thus leading to an increase in the production of soluble complexes [39]. Furthermore, at pH 4.0 due to the superficial negative charge present in solution, reduced electrostatic interaction occurred, resulting in the lowest optical dispersity. In this work, and in accordance with the close to zero ζ-potential value at pH 3, the formation of insoluble complexes was higher (higher optical dispersion values achieved) compared to the other pHs tested. To guarantee that the chosen parameters are already in the maximum interaction region, the optimal λ-CRG/BAE weight ratio of 0.05 and pH 3 was selected for the optimized production of BAE-λ-CRG insoluble complexes.

3.3 | Physicochemical Characterization of the Insoluble Complexes

3.3.1 | Incorporation Rate and Loading Capacity of λ-CRG

To determine the anthocyanins' incorporation rate and the loading capacity of λ-CRG at optimized conditions, insoluble complexes were prepared at pH 3.0 at a λ-CRG/BAE weight ratio of 0.05, and the amount of anthocyanins in the supernatant was analyzed by HPLC-DAD. An incorporation rate of 12±2% was obtained, reflecting the quantity of anthocyanins' molecules that were able to form insoluble complexes with λ-CRG. A loading capacity of 1.1±0.1 g of cy3glc *per* g of λ-CRG was also observed. While anthocyanins are most stable at acid pH values (pH<2), they still show significant stability at pH 3.0. In this sense, reduced degradation should be expected in these experimental conditions. Additionally, anthocyanins and λ-CRG may also form soluble complexes, increasing the total amount of anthocyanins present in the supernatant and easily detected by HPLC-DAD, after complexes disruption. Considering the incorporation rate obtained, about 88% of anthocyanins could be found in the supernatant, both in free or complexed form with λ-CRG. In a similar study, the incorporation rate of *Vaccinium myrtillus* anthocyanins in ι- and κ-CRG was around 1.5 g of anthocyanins *per* g of CRG, close to the values obtained in this work [16]. Furthermore, variations in the incorporation rate were observed considering the changes in the total reagent concentration and weight ratio. The complexation of blueberry anthocyanins with dextran sulfate was also investigated [23], with the results showing that at the ratio of dextran sulfate/ANCs of 1/0.4 and at a total concentration of 0.7 g. L^{-1}, the incorporation rate of ANCs was 74%, while the loading capacity of dextran sulfate was 1.7 g of ANCs *per* g of dextran sulfate. Additionally, using a different approach of stabilization, other authors studied the incorporation of ANCs from *Carissa carandas* in a biopolymer-based coacervate, with chitosan and pectin, and the incorporation rate reported was approximately 48% [29], significantly higher than the values obtained herein. The presence of low molecular weight phenolic compounds and other impurities, such as soluble proteins or sugars, may also affect anthocyanins complexation with λ-CRG. This can occur through anthocyanins interaction, thus reducing the available amount to interact with λ-CRG [40].

3.3.2 | Morphology Analysis: SEM and *Cryo*-SEM

The morphological structure of freeze-dried BAE, λ-CRG, and BAE-λ-CRG insoluble complexes was determined through SEM analysis, as presented in Figure 2.

According to the SEM analysis, BAE showed a dense composition with a wrinkled surface, whereas the morphology of the λ-CRG displayed a considerably smoother surface featuring filamentous and irregular shapes. Additionally, freeze-dried BAE-λ-CRG insoluble complexes, formed at a weight ratio of 0.05 and at pH 3.0, exhibited a homogenous and compact structure with surface pores and a reticular network pattern. The microscopic analysis of these complexes indicated successful complexation, resulting in a distinct network structure, likely attributed to electrostatic interactions between anthocyanin molecules and carrageenan, which seemed to facilitate the formation of a 3D structure, resembling the disorganized structure commonly observed in coacervates as reported in previous literature [11, 41].

To perform the morphological characterization of insoluble complexes' structure in their native environment, studying their intact structure and liquid-like nature, cryo-SEM analysis was also performed. Results are presented in Figure 3 at different magnifications. Cryo-SEM analysis showed that the insoluble complexes exhibited a compact structure with a continuous network, with multiple pores and hollows, typical for hydrogels. This morphology may result from the polyelectrolyte interactions of λ-CRG and BAE during the self-assembly of coacervates in solution. Particularly, the interaction between the positively charged flavylium cation and the negatively charged sulfate groups of λ-CRG may promote the formation of intermolecular association sites that act as physical cross-linking points within the polysaccharide matrix. This allows the development of a 3D polymer network capable of entrapping water and leading to a hydrated gel structure with interconnected pores [42]. A recent study examined the morphology of coacervates formed by pectin and chitosan to encapsulate anthocyanins. Coacervates loaded with anthocyanins did not exhibit micropores, in contrast to the unloaded coacervates [29]. The absence of micropores after encapsulation was attributed to anthocyanins occupying the available spaces within the blank coacervate. Morphological properties of coacervates formed by soybean protein isolate and chitosan were also investigated [43]. The authors proposed that the interaction between the polyelectrolyte complexes resulted in the formation of a network structure resembling pores, similarly to the results obtained herein.

3.3.3 | Structural Elucidation by FTIR-ATR

To evaluate possible interactions between the BAE and λ-CRG and to investigate differences in the functional groups of the produced insoluble complexes, Fourier Transform Infrared Spectroscopy with attenuated total reflection (FTIR-ATR) analysis was performed (Figure 4).

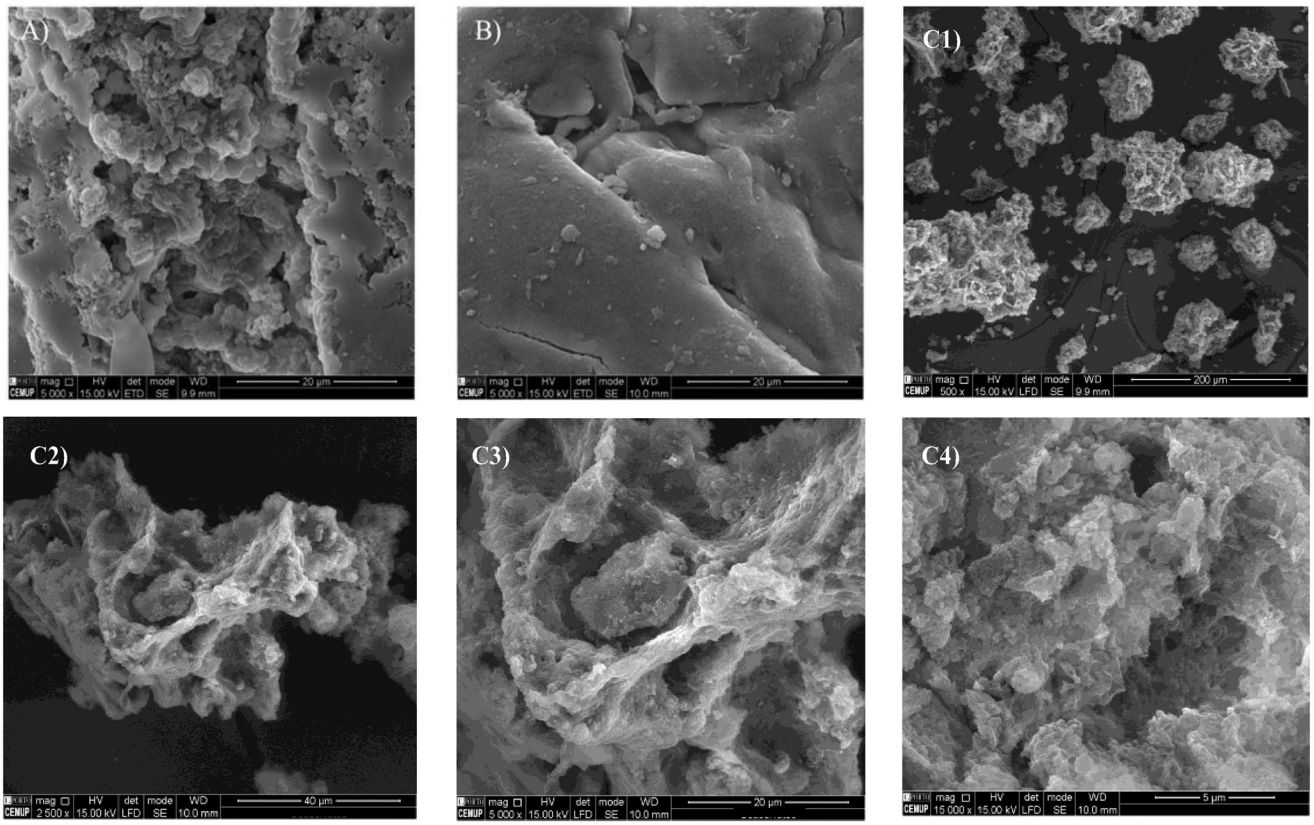

FIGURE 2 | Scanning electron microscopy (SEM) images of A) BAE and B) λ-CRG (magnification 5000x, scale bar = 20 μm). Scanning electron microscopy (SEM) images of BAE-λ-CRG insoluble complexes at different magnifications (C1: magnification 500x, scale bar = 200 μm; C2: magnification 2500x, scale bar = 40 μm; C3: magnification 5000x, scale bar = 20 μm; C4: magnification 15000x, scale bar = 5 μm).

For comparison, lyophilized BAE and λ-CRG were also analyzed.

The FTIR-ATR spectra analysis of BAE revealed several significant groups [44]. The BAE exhibited a broad O-H stretch band at 3234 cm^{-1}, indicative of -OH bond vibrations. The presence of a stretching vibration of C-H bonds was identified at 2915 cm^{-1}, while a band at 1730 cm^{-1} was attributed to the stretching vibration of C = O in the benzopyran aromatic ring in the anthocyanins' skeleton molecule. The absorption band at 1643 cm^{-1} and the bands at 1518 and 1446 cm^{-1} were attributed to stretching vibrations and the deformation vibration, respectively, of the two phenyl rings. In addition, the band at 1280 cm^{-1} was attributed to the C-O vibration in anthocyanins' aromatic rings. Similarly, the FTIR-ATR spectrum of λ-CRG displayed a broad O-H stretch band at 3400 cm^{-1}, corresponding to -OH groups. The bands at 1217 and at 842 cm^{-1} were assigned, respectively, to the O = S = O symmetric vibration and to the C-O-S stretching vibration of galactose-4-sulfate [1, 16]. In the spectrum of BAE-λ-CRG insoluble complexes, the dominant bands of the anthocyanic extract combined with the spectra of λ-CRG were detected. A stretching vibration of the OH bond was observed at 3251 cm^{-1}, possibly indicating hydrogen bonding resulting from the interaction between ANCs and λ-CRG. The stretching vibration of the C = O bond in the benzopyran ring was also identified in the BAE-λ-CRG complexes, albeit at a higher wavenumber, which can be attributed to the interaction with λ-CRG molecules. Furthermore, the band corresponding to the O = S = O symmetric vibration was shifted to lower wavelengths (1193 cm^{-1}). This behavior suggests the occurrence of complexation, likely due to electrostatic interactions between the positively charged anthocyanin flavylium cation and the negatively charged sulfate groups of CRG. A similar behavior was observed in a study on the complexation of anthocyanins from blueberries with CRG [16].

3.4 | Thermal Stability Studies

The thermal stability of BAE, λ-CRG, and the BAE-λ-CRG complexes was obtained by thermogravimetry analysis (TGA). The mass loss thermogravimetry (TG) and its corresponding derivative thermogravimetric curves (DTG, inset in Figure 5), at 5°C/min scanning rate, are shown in Figure 5. As observed in this figure, with the temperature increase, a significant increase in mass loss was observed. BAE exhibited rapid degradation with the temperature increase, with a total mass loss of 44%. Two degradation phases were observed: the first occurred at approximately 50°C (≈10 min), corresponding to water loss (7% weight loss), while the second phase occurred around 193°C (≈38 min), attributed to anthocyanins degradation (37% weight loss). The DTG data indicated a peak temperature (T_{peak}) for maximum degradation at 194°C. A similar two-phase degradation behavior at comparable temperatures was observed in a previous study on the thermal degradation of cy3glc [45]. The λ-CRG also exhibited two stages of degradation, with a total weight loss of 53%. The first phase occurred at around 50°C (≈ 10 min),

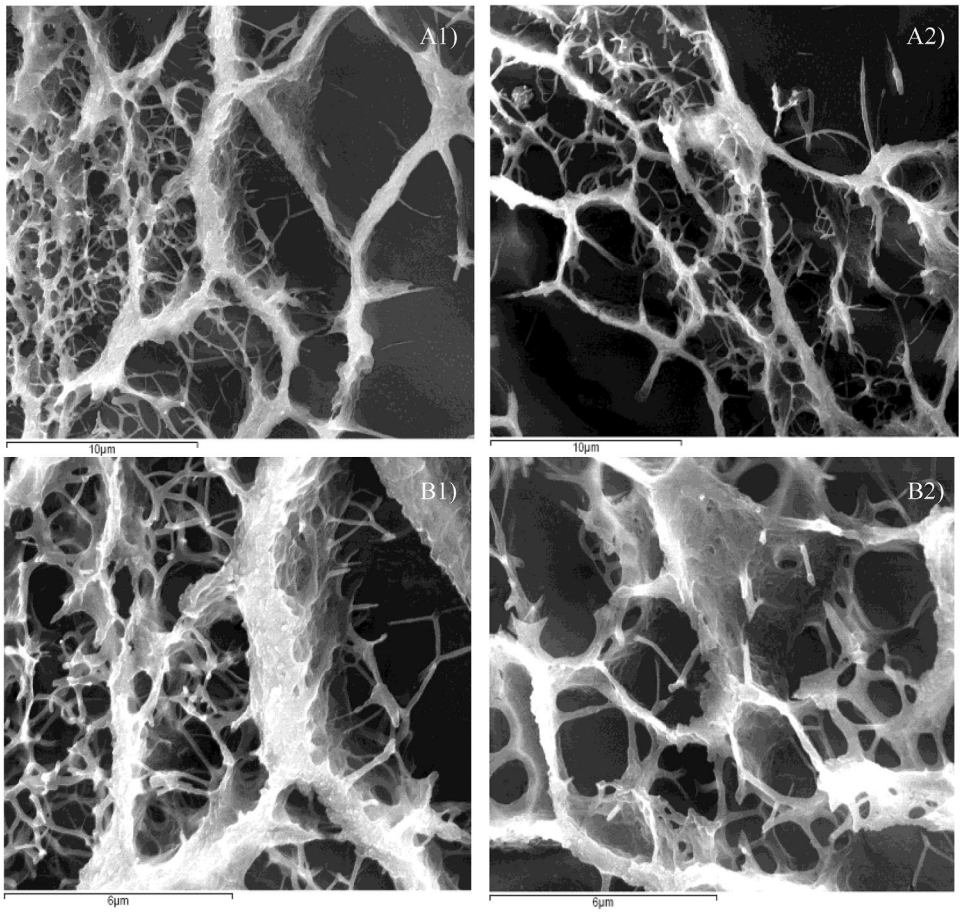

FIGURE 3 | Cryo-scanning electron microscopy (cryo-SEM) images of wet BAE-λ-CRG insoluble complexes (prepared at a mass ratio of 0.05) at different magnifications (A1 and A2, magnification 5000x, scale bar = 10 µm; B1 and B2, magnification 10000x, scale bar = 6 µm). The accelerating voltage was 15 kV and the working distance of 15 mm in all cases.

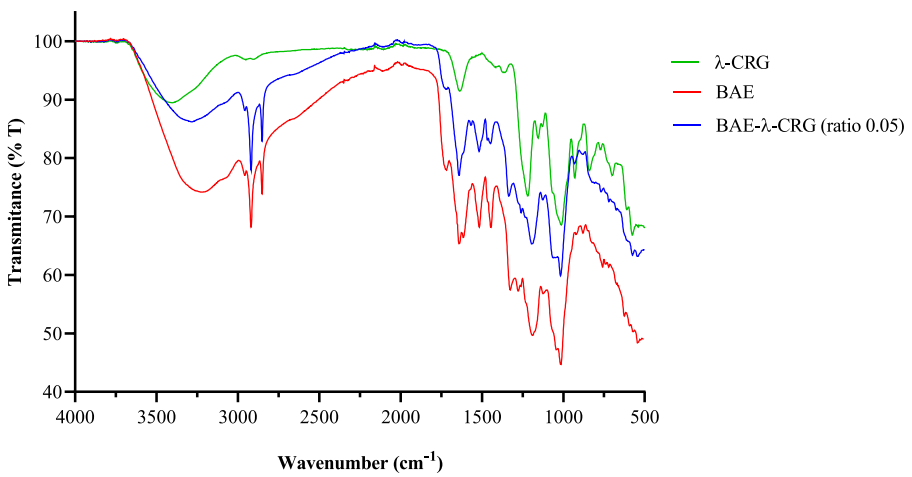

FIGURE 4 | FTIR-ATR spectra of the BAE, λ-CRG, and BAE-λ-CRG insoluble complexes (prepared at a mass ratio of 0.05).

corresponding to 11% weight loss, which could be attributed to water loss trapped in the λ-CRG molecules. This behavior was consistent with previous TGA studies on λ-carrageenan [46]. The second phase occurred at 230°C (≈ 46 min) and resulted in 36% weight loss, associated with the removal of sulfate groups from the main polygalactan structure, followed by the degradation of the carbohydrate backbone. The onset temperature of thermal degradation (T_{onset}) was observed at approximately 200°C, while the T_{peak} was observed at 225°C. The insoluble BAE-λ-CRG complexes (prepared at the optimum weight ratio of 0.05)

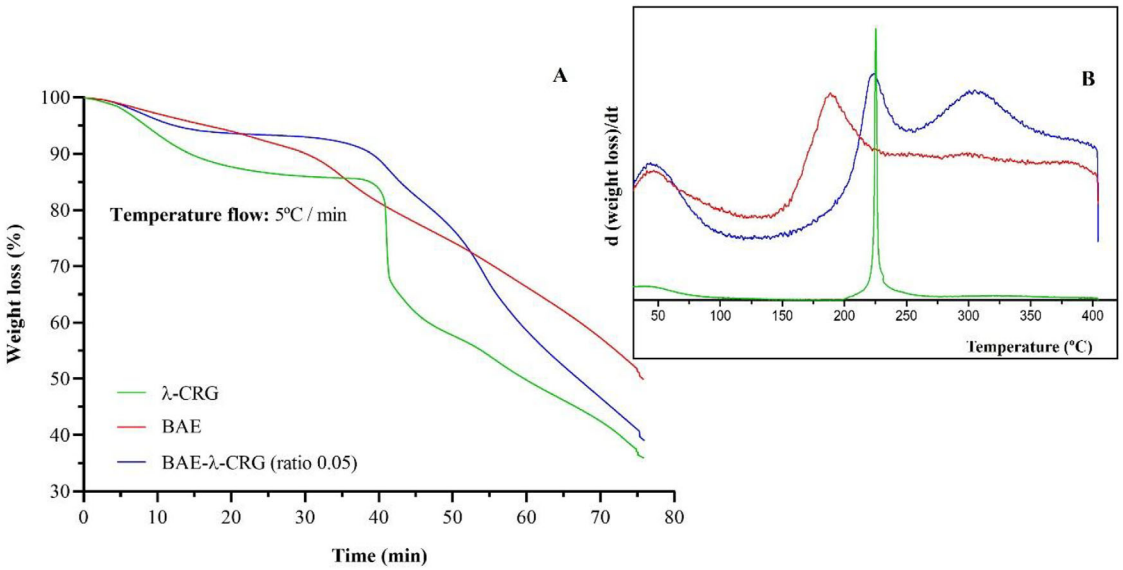

FIGURE 5 | Thermogravimetric analysis (TGA) (A) thermogram and derivative thermogravimetry curve (DTG) (inset graphic—B) for the thermal decomposition of BAE, λ-CRG, and BAE-λ-CRG insoluble complexes (prepared at a mass ratio of 0.05), at $\beta = 5°C.min^{-1}$.

exhibited two phases of degradation with similar temperatures and weight loss values as the BAE thermogram. The first stage of degradation occurred around 50°C, resulting in 7% weight loss, attributed to moisture evaporation. The second stage of degradation occurred at 225°C and was likely related to the removal of sulfite groups from the λ-CRG molecule. The T_{onset} remained the same as the BAE profile (160°C), but the T_{peak} shifted to a higher temperature at 225°C. The TGA profile of the BAE-λ-CRG complexes resembled that of the BAE, but the rapid degradation plateau occurred at higher temperatures. Moreover, the T_{peak} was higher (31°C) compared to the BAE, suggesting improved thermal stability due to the molecular complexation. According to the FTIR analysis, electrostatic interactions between the positively charged flavylium cation and the negatively charged λ-CRG sulfate groups, together with hydrogen bonding, may be responsible for this molecular complexation and subsequent thermal stabilization. Another study, using zedo gum and gelatin to encapsulate anthocyanins also demonstrated enhanced thermal stability in the formed coacervates compared to free zedo gum, attributed to stronger interactions between gelatin and zedo gum [47]. In this case, the improved thermal stability may be associated with the incorporation of λ-CRG.

Figure 6 shows the DSC curves of all three systems. The DSC data of BAE exhibited two endothermic peaks: one ranging from 50°C to 100°C and another from 163°C to 202°C. λ-CRG displayed a prominent exothermic peak from 206°C to 233°C, likely associated with the polysaccharide's melting point. The BAE-λ-CRG insoluble complexes showed two endothermic peaks, with the first occurring at the same temperature as the peak observed at BAE. The second endothermic peak aligned with the temperature range of the λ-CRG peak, suggesting a transitional phase present in the λ-CRG sample. Notably, the second endothermic peak observed in the BAE was absent in the thermogram of the mixture, indicating enhanced thermal stability of the anthocyanins in the extract and successful complexation. A study investigating blackberry anthocyanins encapsulated in β-cyclodextrin demonstrated improved thermal stability, with the same endothermic peak in the BAE shifting to higher temperatures, similar to the behavior observed for the produced insoluble complexes [31]. In summary, the thermal analysis provided valuable insights into the behavior and stability of the BAE, λ-CRG, and BAE-λ-CRG complexes. The results demonstrated improved thermal stability in the complexes and indicated successful complexation, as evidenced by shifts in peak temperatures and weight loss profiles compared to the individual components.

3.5 | Release Pattern: Desorption Studies

Anthocyanins release pattern from λ-CRG-based insoluble complexes was studied in water at three pH values (pH 1.7, 5.4, and 7.4), or in buffer solutions (10 mM MES or PBS buffer),. The purpose of this assay, in two different medium, was to evaluate the release pattern of anthocyanins in a range of pHs from acidic to neutral conditions and to test the influence of salts. Anthocyanins' cumulative release rate is presented in Figure 7. After the suspension of BAE-λ-CRG complexes in each medium, the initial anthocyanins burst release could be observed, with this release being more noticeable in PBS buffer (16.5 ± 2.4%), followed by water medium at pH = 1.7 (5.6 ± 0.4%), pH = 5.4 (2.6 ± 0.3%), and pH = 7.4 (2.4 ± 0.1%). The lowest initial release was observed in MES, at pH 5.4 (1.8 ± 0.1%). This early release is in accordance with the color of the respective samples at the 0-hour mark (Figure 7), suggesting the burst release of anthocyanins present on the surface of the polymer. The results of the cumulative release percentage at each hour (expressed as a percentage of anthocyanins release compared to the initial release—t 0 h) showed that at pH 5.4, both in ultrapure water and MES, the release of anthocyanins reached a plateau after 1 h of study, with a maximum of anthocyanins release around 5%, thus suggesting that there was no significant impact of salts present in the buffer on anthocyanins desorption mechanism at pH 5.4. Additionally, at this pH, it seems that the release of

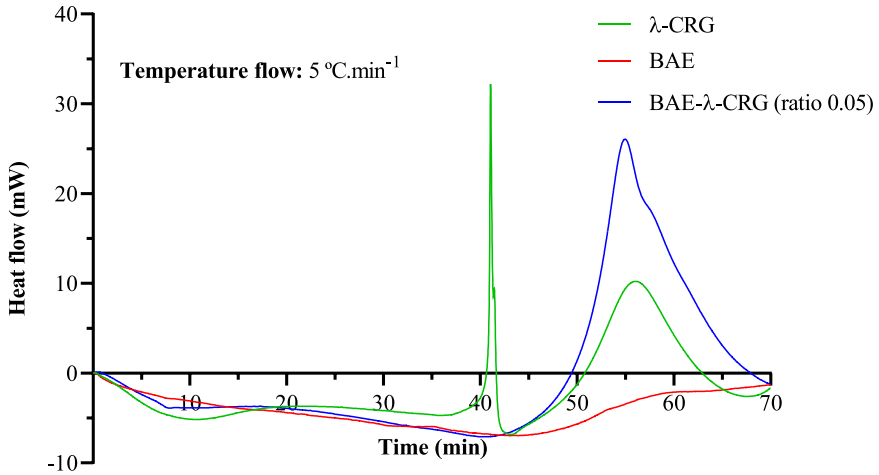

FIGURE 6 | DSC thermograms of BAE, λ-CRG, and BAE-λ-CRG insoluble complexes (prepared at a mass ratio of 0.05), at $\beta = 5°C.min^{-1}$.

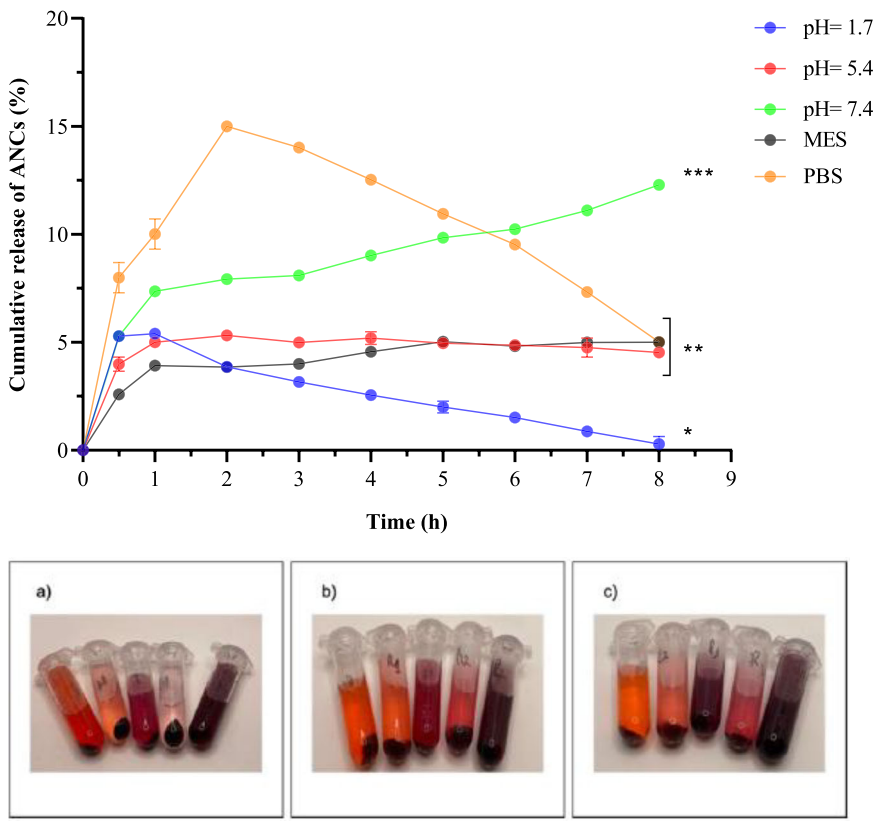

FIGURE 7 | Percentage of cumulative release of anthocyanins from BAE-λ-CRG insoluble complexes (prepared at a mass ratio of 0.05) versus time at pH 1.7, 5.4, and 7.4 (in ultrapure water, MES, and PBS buffer). At the 8-hour mark, samples with the same symbol are not statistically different ($p>0.05$). On the bottom, color of the samples in the ANCs release pattern study. From left to right in all pictures: pH = 1.7, pH = 5.4, pH = 7.4, MES, and PBS. a) t = 0 h; b) t = 4 h; c) t = 8 h.

anthocyanins achieved an equilibrium between the contribution of the rate of diffusion of anthocyanins and the dilution factor at each time point. The highest release rate for anthocyanins was recorded at pH 7.4, both in PBS and ultrapure water. In PBS, a maximum release of about 15% was observed after the 2-hour mark, thus suggesting the most pronounced disruption of the BAE-λ-CRG complexes under these conditions. After this period, a sharp decrease in anthocyanins' cumulative release could be observed, possibly due to the rapid degradation of anthocyanins in PBS medium. At pH>2 anthocyanins degradation is due to the reversible water addition to the flavylium ion (with concomitant accumulation of a colorless hemiketal and pale yellow *cis*- and *trans*-chalcones) and to a combination of irreversible routes (hydrolytic and oxidative pathways) typically resulting in cleavage of the C-ring [48]. Moreover, the presence of salts can also accelerate the irreversible degradation of anthocyanins, possibly

due to the altered solvation characteristics of aqueous solutions [49]. On the other hand, after this timepoint, anthocyanins dilution, due to solvent replacement may also contribute to this decrease, being higher than anthocyanins' diffusion. In ultrapure water at pH 7.4, anthocyanins' release showed a continuous increase until the end of the assay, reaching a maximum of 12% at 8 h. In this medium, and on the opposite to what was observed in PBS buffer, a reduced degradation could be observed combined with a continuous release. At pH 1.7, the maximum of release was observed between 0.5-1.0 h mark (around 6%), followed by a decrease in the cumulative percentage release. This decline suggests that the effect sample dilution, when small aliquots were removed, was higher than the diffusion of anthocyanins from the insoluble complexes, as observed for the lighter color presented at the end of the experiment. In contrast to these results, Sarkar et al., reported a higher release of anthocyanins at acidic pH when encapsulated in chitosan-pectin coacervates. Furthermore, at pH 7, the lowest percentage of anthocyanins was observed (around 40%) [29].

The obtained release data at different pH values were fitted with the Korsmeyer-Peppas model, considering the diffusion of water into the polymeric system, the swelling of the polymeric chain, and the dissolution of anthocyanins [50] (Figure S1). Despite its limitations, particularly for porous hydrogel networks, the Korsmeyer–Peppas model is widely used [51]. This model is commonly applied to the initial stage of release (typically up to approximately 60% of the total drug released), while for porous materials, drug release may involve multi-stage kinetics, including burst release, diffusion, and polymeric matrix relaxation. Furthermore, it does not take into consideration the pore size distribution and the quantity, and therefore, it cannot distinguish between a dense or porous network or quantify the impact of porous structure for the transport. Moreover, this model assumes idealized geometries (e.g. slabs, cylinders, or spheres) and homogeneous matrices, conditions that are not strictly fulfilled in porous hydrogel matrices. Therefore, the structural heterogeneity of the hydrogel network may introduce deviations from the theoretical assumptions of the model. Consequently, although the porous and heterogeneous structure of hydrogels does not fully satisfy the ideal assumptions of the model, the Korsmeyer–Peppas equation was employed in this study as a simplified empirical tool to obtain an indicative interpretation of the dominant drug release mechanism, rather than as a rigorous mechanistic description of transport within the porous hydrogel network.

Data obtained in PBS and at pH 1.7 were not considered due to the decrease in the cumulative amount of anthocyanins, not allowing the application of the Korsmeyer-Peppas model. Although the plotted data showed a good coefficient of determination ($R^2 >$ 0.98), suggesting a good fit, while the n-values calculated from the curves allowed us to determine how the release occurred under the diffusion law of Fick. The Fickian diffusion mechanism describes the time of a transfer of solutes when a gradient of concentration is obtained [52]. In this case, the release can be dominated by phenomena of diffusion and rearrangement of polymeric chains. The release of anthocyanins by diffusion happens when water enters the surface of the polymeric system, it swells, and the anthocyanins are dissolved and removed from the complex structure by diffusion. Thus, the swelling rate at which anthocyanins leave the polymeric system determines how the release behaves [53]. For this, following the Korsmeyer-Peppas model, the determination of n defines the type of transport. For spherical delivery systems, when $n < 0.43$, the release follows Fick's law, mainly caused by diffusion. On the other hand, if $n = 0.85$, the transport of solutes follows the zero law of kinetics. Finally, if $0.43 < n < 0.85$, the release is considered a case II transport, mainly caused by diffusion and swelling, which may indicate that the release is mainly dependent on time (non-Fickian transport) [54]. In water, the n value for anthocyanins release ranged from 0.05 and 0.26 for pH 5.4 and 7.4, respectively. At pH 5.4 (MES), the n value was around 0.21. All these values are below the threshold of $n \leq 0.43$, accepted in polydisperse microparticles [55], which indicates that in these conditions the release follows a Fickian diffusion mechanism [56], suggesting that when the water enters the polymeric matrix, the rate of anthocyanins' diffusion was higher than the rate of polymeric relaxation.

4 | Conclusion

In this study, the optimized formation of bioPECs based on an anionic polysaccharide (λ-CRG) and anthocyanins, was achieved. The ideal weight ratio for insoluble bioPECs formation was 0.05 (λ-CRG/BAE), at pH 3.0. Dried insoluble complexes displayed an irregular and porous shape, with a compact structure. In wet form, the BAE-λ-CRG complexes exhibited a hydrogel-like morphology. The FTIR-ATR confirmed the complexation between blackberries' anthocyanins and the λ-CRG, mainly through electrostatic interactions, which induced a thermal stabilization, with higher temperatures observed for the degradation in the BAE-λ-CRG insoluble complexes. The release studies showed that the formulations of bioPECs presented a low percentage of anthocyanins released for 8 h, with this being dependent on the pH of the medium. Anthocyanin-polysaccharide insoluble polyelectrolyte complexes represent a significant advancement in stabilizing anthocyanins, providing functional properties for real-world and high-value applications, such as food packaging, monitoring food freshness while preventing anthocyanins from dissolving into the food, or significantly improving the color retention of anthocyanin-based food ingredients during thermal processing and storage, and boosting stability in the gastrointestinal tract.

Author Contributions

Tomás Garrido: Investigation, Data curation, Formal analysis, Writing – original draft. **Ana Rita Pereira**: Methodology, Investigation. **Hiléia K.S. Souza**: Methodology, Visualization, Investigation. **Nuno Mateus**: Visualization, Writing – review & editing. Victor de Freitas: Funding Acquisition, Writing – review & editing. **Ana Fernandes**: Conceptualization, Supervision, Formal analysis, Writing – review & editing.

Acknowledgments

This work received financial support from the PT national funds (FCT/MECI, Fundação para a Ciência e Tecnologia and Ministério da Educação, Ciência e Inovação) through the project UID/50006/2025 DOI 10.54499/UID/50006/2025 -Laboratório Associado para a Química

Verde—Tecnologias e Processos Limpos. Ana Fernandes (AF) acknowledges Fundação para a Ciência e Tecnologia (FCT) for the research contract 2023.14741.TENURE.006/CP00058/CT00009. The authors acknowledge the technical support of CEMUP and FCUP | DQB-Lab & Services in Porto University, Portugal.

Conflicts of Interest

All authors declare that they have no known competing financial interests or personal relationships that could have appeared to influence the work reported in this paper.

References

1. C. T. Nthimole, T. Kaseke, and O. A. Fawole, "Exploring the Extraction and Application of Anthocyanins in Food Systems," *Processes* 12 (2024): 2444, https://doi.org/10.3390/pr12112444.

2. P. Trouillas, J. C. Sancho-García, V. De Freitas, J. Gierschner, M. Otyepka, and O. Dangles, "Stabilizing and Modulating Color by Copigmentation: Insights From Theory and Experiment," *Chemical Reviews* 116 (2016): 4937–4982, https://doi.org/10.1021/acs.chemrev.5b00507.

3. H. E. Khoo, A. Azlan, S. T. Tang, and S. M. Lim, "Anthocyanidins and Anthocyanins: Colored Pigments as Food, Pharmaceutical Ingredients, and the Potential Health Benefits," *Food & Nutrition Research* 61 (2017): 1361779, https://doi.org/10.1080/16546628.2017.1361779.

4. C. Santos-Buelga, N. Mateus, and V. De Freitas, "Anthocyanins. Plant Pigments and beyond," *Journal of Agricultural and Food Chemistry* 62 (2014): 6879–6884, https://doi.org/10.1021/jf501950s.

5. Y. Jaouhari, W. Tao, V. Disca, et al., "Encapsulation of Anthocyanins: A Key for Improvement of the Gut-metabolism Health Axis?," *Food Research International* 221 (2025): 117380, https://doi.org/10.1016/j.foodres.2025.117380.

6. B. Salehi, J. Sharifi-Rad, F. Cappellini, et al., "The Therapeutic Potential of Anthocyanins: Current Approaches Based on Their Molecular Mechanism of Action," *Frontiers in Pharmacology* 11 (2020): 2020.

7. L. V. Srinivasan and S. S. Rana, "Anthocyanins: A Promising Source of Natural Colorants and Nutraceuticals," *Discover Applied Sciences* 7 (2025): 694, https://doi.org/10.1007/s42452-025-07196-7.

8. D. Fraisse, A. Bred, C. Felgines, and F. Senejoux, "Stability and Antiglycoxidant Potential of Bilberry Anthocyanins in Simulated Gastrointestinal Tract Model," *Foods* 9 (2020): 1695.

9. H. Xue, J. Zhao, Y. Wang, et al., "Factors Affecting the Stability of Anthocyanins and Strategies for Improving Their Stability: A Review," *Food Chemistry: X* 24 (2024): 101883.

10. Y. Yuan, Q. Fan, X. Xu, O. Wang, L. Zhao, and L. Zhao, "Nanocarriers Based on Polysaccharides for Improving the Stability and Bioavailability of Anthocyanins: A Review," *Carbohydrate Polymer Technologies and Applications* 6 (2023): 100346, https://doi.org/10.1016/j.carpta.2023.100346.

11. V. S. Meka, M. K. G. Sing, M. R. Pichika, S. R. Nali, V. R. M. Kolapalli, and P. Kesharwani, "A Comprehensive Review on Polyelectrolyte Complexes," *Drug Discovery Today* 22 (2017): 1697–1706, https://doi.org/10.1016/j.drudis.2017.06.008.

12. C. Tan, M. Huang, J. Wang, and B. Sun, "Biopolyelectrolyte Complex (bioPEC)-Based Carriers for Anthocyanin Delivery," *Food Hydrocolloids for Health* 1 (2021): 100037, https://doi.org/10.1016/j.fhfh.2021.100037.

13. C. Tan, Y. Sun, X. Yao, et al., "Stabilization of Anthocyanins by Simultaneous Encapsulation-Copigmentation via Protein-Polysaccharide Polyelectrolyte Complexes," *Food Chemistry* 416 (2023): 135732, https://doi.org/10.1016/j.foodchem.2023.135732.

14. S. S. Rosales-Murillo, J. Sánchez-Bodón, S. L. Hernández Olmos, et al., "Anthocyanin-Loaded Polymers as Promising Nature-Based, Responsive, and Bioactive Materials," *Polymers* 16 (2024): 163, https://doi.org/10.3390/polym16010163.

15. W. Tao, I. M. P. L. V. O. Ferreira, J. He, et al., "Tailored Zein-Polysaccharide Nanoparticles for Anthocyanin Encapsulation: Insights Into Preparation and Characterization," *Food Hydrocolloids* 166 (2025): 111365, https://doi.org/10.1016/j.foodhyd.2025.111365.

16. V. Navikaite, D. Simanaviciute, R. Klimaviciute, V. Jakstas, and L. Ivanauskas, "Interaction Between *κ*- and *ι*-carrageenan and Anthocyanins From Vaccinium myrtillus," *Carbohydrate Polymers* 148 (2016): 36–44, https://doi.org/10.1016/j.carbpol.2016.04.059.

17. A. F. Thünemann, M. Müller, H. Dautzenberg, J.-F. Joanny, and H. Löwen, *Polyelectrolytes With Defined Molecular Architecture II*, ed. M. Schmidt, (Springer, 2004), 113–171.

18. R. Kubota, "A Minimalist Design Approach to Simple Coacervates From Low-Molecular-Weight Components," *Polymer Journal* 57 (2025): 815–829, https://doi.org/10.1038/s41428-025-01037-5.

19. J. K. Bediako, E. S. M. Mouele, Y. El Ouardi, and E. Repo, "Saloplastics and the Polyelectrolyte Complex Continuum: Advances, Challenges and Prospects," *Chemical Engineering Journal* 462 (2023): 142322, https://doi.org/10.1016/j.cej.2023.142322.

20. A. Fernandes, F. Raposo, D. V. Evtuguin, et al., "Grape Pectic Polysaccharides Stabilization of Anthocyanins Red Colour: Mechanistic Insights," *Carbohydrate Polymers* 255 (2021): 117432, https://doi.org/10.1016/j.carbpol.2020.117432.

21. C. Shi, C. Guo, S. Wang, et al., "The Mechanism of Pectin in Improving Anthocyanin Stability and the Application Progress of Their Complexes: A Review," *Food Chemistry: X* 24 (2024): 101955.

22. J. Song, Y. Yu, M. Chen, et al., "Advancement of Protein- and Polysaccharide-Based Biopolymers for Anthocyanin Encapsulation," *Frontiers in Nutrition* 9 (2022): 938829, https://doi.org/10.3389/fnut.2022.938829.

23. R. Klimaviciute, V. Navikaite, V. Jakstas, and L. Ivanauskas, "Complexes of Dextran Sulfate and Anthocyanins From Vaccinium myrtillus: Formation and Stability," *Carbohydrate polymers* 129 (2015): 70–78, https://doi.org/10.1016/j.carbpol.2015.04.038.

24. D. Jeong and K. Na, "Chondroitin Sulfate Based Nanocomplex for Enhancing the Stability and Activity of Anthocyanin," *Carbohydrate Polymers* 90 (2012): 507–515, https://doi.org/10.1016/j.carbpol.2012.05.072.

25. A. Martín-del-Campo, J. A. Fermín-Jiménez, V. V. Fernández-Escamilla, Z. Y. Escalante-García, M. E. Macías-Rodríguez, and Y. Estrada-Girón, "Improved Extraction of Carrageenan From Red Seaweed (Chondracantus canaliculatus) Using Ultrasound-assisted Methods and Evaluation of the Yield, Physicochemical Properties and Functional Groups," *Food Science and Biotechnology* 30 (2021): 901–910, https://doi.org/10.1007/s10068-021-00935-7.

26. V. L. Singleton and J. A. Rossi, "Colorimetry of Total Phenolics With Phosphomolybdic-Phosphotungstic Acid Reagents," *American journal of enology and viticulture* 16 (1965): 144–158, https://doi.org/10.5344/ajev.1965.16.3.144.

27. N. J. Kruger, *The Protein Protocols Handbook*, ed. J. M. Walker, (Humana Press, 2009), 17–24.

28. L. Tavares, H. K. S. Souza, M. P. Gonçalves, and C. M. R. Rocha, "Physicochemical and Microstructural Properties of Composite Edible Film Obtained by Complex Coacervation Between Chitosan and Whey Protein Isolate," *Food Hydrocolloids* 113 (2021): 106471, https://doi.org/10.1016/j.foodhyd.2020.106471.

29. R. Sarkar, A. Dutta, A. Patra, and S. Saha, "Bio-Inspired Biopolymeric Coacervation for Entrapment and Targeted Release of Anthocyanin," *Cellulose* 28 (2021): 377–388, https://doi.org/10.1007/s10570-020-03523-w.

30. W. Zhu, J. Long, and M. Shi, "Release Kinetics Model Fitting of Drugs With Different Structures From Viscose Fabric," *Materials* 16 (2023): 3282, https://doi.org/10.3390/ma16083282.

31. A. Fernandes, M. A. A. Rocha, L. M. N. B. F. Santos, et al., "Blackberry Anthocyanins: B-Cyclodextrin Fortification for Thermal and

Gastrointestinal Stabilization," *Food Chemistry* 245 (2018): 426–431, https://doi.org/10.1016/j.foodchem.2017.10.109.

32. F. Marques Peixoto, I. Fernandes, A. C. M. S. Gouvêa, et al., "Simulation of in Vitro Digestion Coupled to Gastric and Intestinal Transport Models to Estimate Absorption of Anthocyanins From Peel Powder of Jabuticaba, Jamelão and Jambo Fruits," *Journal of Functional Foods* 24 (2016): 373–381, https://doi.org/10.1016/j.jff.2016.04.021.

33. H. Chen, H.-F. Zhao, X.-H. Meng, et al., "Effect of Blackberry Anthocyanins and its Combination With Tea Polyphenols on the Oxidative Stability of Lard and Olive Oil," *Frontiers in Nutrition* 10 (2023): 2023.

34. L. Cruz, N. Mateus, and V. de Freitas, "pH-Regulated Interaction Modes Between Cyanidin-3-Glucoside and Phenylboronic Acid-Modified Alginate," *Carbohydrate Polymers* 280 (2022): 119029, https://doi.org/10.1016/j.carbpol.2021.119029.

35. F. Jabeen, A. Zil, R. Ahmad, S. Mir, N. S. Awwad, and H. A. Ibrahium, "Carrageenan: Structure, Properties and Applications With Special Emphasis on Food Science," *RSC Advances* 15 (2025): 22035–22062, https://doi.org/10.1039/D5RA03296B.

36. E. S. Dragan and S. Schwarz, "Polyelectrolyte Complexes. VI. Polycation Structure, Polyanion Molar Mass, and Polyion Concentration Effects on Complex Nanoparticles Based on Poly(sodium 2-acrylamido-2-methylpropanesulfonate)," *Journal of Polymer Science Part A: Polymer Chemistry* 42 (2004): 2495–2505, https://doi.org/10.1002/pola.20110.

37. L. Seres, E. Csapó, N. Varga, and Á. Juhász, "The Effect of Concentration, Temperature, and pH on the Formation of Hyaluronic Acid–Surfactant Nanohydrogels," *Gels* 9 (2023): 529, https://doi.org/10.3390/gels9070529.

38. C. Tapia, Z. Escobar, E. Costa, et al., "Comparative Studies on Polyelectrolyte Complexes and Mixtures of Chitosan–Alginate and Chitosan–Carrageenan as Prolonged Diltiazem Clorhydrate Release Systems," *European Journal of Pharmaceutics and Biopharmaceutics* 57 (2004): 65–75, https://doi.org/10.1016/S0939-6411(03)00153-X.

39. H. Espinosa-Andrews, K. E. Enríquez-Ramírez, E. García-Márquez, C. Ramírez-Santiago, C. Lobato-Calleros, and J. Vernon-Carter, "Interrelationship Between the Zeta Potential and Viscoelastic Properties in Coacervates Complexes," *Carbohydrate Polymers* 95 (2013): 161–166, https://doi.org/10.1016/j.carbpol.2013.02.053.

40. O. Dangles and J.-A. Fenger, "The Chemical Reactivity of Anthocyanins and Its Consequences in Food Science and Nutrition," *Molecules (Basel, Switzerland)* 23 (2018): 1970, https://doi.org/10.3390/molecules23081970.

41. S. Muñoz-Coyotecatl, A. Domínguez-Uscanga, R. Ortiz-Castro, et al., "Complex Coacervation of Anthocyanin-Rich Pigments From Red Cabbage (Brassica Oleracea) With Inulin, Gum Arabic and Pea Protein," *Frontiers in Nutrition* 12 (2025): 2025.

42. X. T. Le, L.-E. Rioux, and S. L. Turgeon, "Formation and Functional Properties of Protein–Polysaccharide Electrostatic Hydrogels in Comparison to Protein or Polysaccharide Hydrogels," *Advances in Colloid and Interface Science* 239 (2017): 127–135, https://doi.org/10.1016/j.cis.2016.04.006.

43. G. Q. Huang, Y. T. Sun, J. X. Xiao, and J. Yang, "Complex Coacervation of Soybean Protein Isolate and Chitosan," *Food Chemistry* 135 (2012): 534–539, https://doi.org/10.1016/j.foodchem.2012.04.140.

44. S. Ren, L. Rodriguez-Saona, and M. M. Giusti, "Analyzing the Interaction Between Anthocyanins and Native or Heat-Treated Whey Proteins Using Infrared Spectroscopy," *Molecules (Basel, Switzerland)* 27 (2022): 1538, https://doi.org/10.3390/molecules27051538.

45. H. K. S. Souza, N. Mateus, V. de Freitas, M. P. Gonçalves, and L. Cruz, "Chemical/Color Stability and Rheological Properties of Cyanidin-3-Glucoside in Deep Eutectic Solvents as a Gateway to Design Task-Specific Bioactive Compounds," *ACS Sustainable Chemistry & Engineering* 8 (2020): 16184–16196, https://doi.org/10.1021/acssuschemeng.0c04839.

46. F. N. Jumaah, N. N. Mobarak, A. Ahmad, M. A. Ghani, and M. Y. A. Rahman, "Derivative of Iota-Carrageenan as Solid Polymer Electrolyte," *Ionics* 21 (2015): 1311–1320, https://doi.org/10.1007/s11581-014-1306-x.

47. H. Gharanjig, K. Gharanjig, G. Farzi, M. Hosseinnezhad, and S. M. Jafari, "Novel Complex Coacervates Based on Zedo Gum, Cress Seed Gum and Gelatin for Loading of Natural Anthocyanins," *International Journal of Biological Macromolecules* 164 (2020): 3349–3360, https://doi.org/10.1016/j.ijbiomac.2020.08.218.

48. J.-A. Fenger, R. J. Robbins, T. M. Collins, and O. Dangles, "The Fate of Acylated Anthocyanins in Mildly Heated Neutral Solution," *Dyes and Pigments* 178 (2020): 108326, https://doi.org/10.1016/j.dyepig.2020.108326.

49. E. M. Hubbermann, A. Heins, H. Stöckmann, and K. Schwarz, "Influence of Acids, Salt, Sugars and Hydrocolloids on the Colour Stability of Anthocyanin Rich Black Currant and Elderberry Concentrates," *European Food Research and Technology* 223 (2006): 83–90, https://doi.org/10.1007/s00217-005-0139-2.

50. R. W. Korsmeyer, R. Gurny, E. Doelker, P. Buri, and N. A. Peppas, "Mechanisms of Solute Release From Porous Hydrophilic Polymers," *International Journal of Pharmaceutics* 15 (1983): 25–35, https://doi.org/10.1016/0378-5173(83)90064-9.

51. S. Erikci, N. van den Bergh, and H. Boehm, "Kinetic and Mechanistic Release Studies on Hyaluronan Hydrogels for Their Potential Use as a pH-Responsive Drug Delivery Device," *Gels* 10 (2024): 731–746, https://doi.org/10.3390/gels10110731.

52. J. Siepmann and F. Siepmann, "Modeling of Diffusion Controlled Drug Delivery," *Journal of Controlled Release* 161 (2012): 351–362, https://doi.org/10.1016/j.jconrel.2011.10.006.

53. N. A. Khan, A. Khan, R. Ullah, et al., "Preparation and Characterization of Hydrophilic Polymer Based Sustained-Release Matrix Tablets of a High Dose Hydrophobic Drug," *Polymers* 14 (2022): 1985, https://doi.org/10.3390/polym14101985.

54. P. L. Ritger and N. A. Peppas, "A Simple Equation for Description of Solute Release I. Fickian and Non-fickian Release From Non-swellable Devices in the Form of Slabs, Spheres, Cylinders or Discs," *Journal of Controlled Release* 5 (1987): 23–36, https://doi.org/10.1016/0168-3659(87)90034-4.

55. J. M. Unagolla and A. C. Jayasuriya, "Drug Transport Mechanisms and in Vitro Release Kinetics of vancomycin Encapsulated Chitosan-Alginate Polyelectrolyte Microparticles as a Controlled Drug Delivery System," *European Journal of Pharmaceutical Sciences* 114 (2018): 199–209, https://doi.org/10.1016/j.ejps.2017.12.012.

56. J. Supramaniam, R. Adnan, N. H. Mohd Kaus, and R. Bushra, "Magnetic Nanocellulose Alginate Hydrogel Beads as Potential Drug Delivery System," *International Journal of Biological Macromolecules* 118 (2018): 640–648, https://doi.org/10.1016/j.ijbiomac.2018.06.043.

Supporting Information

Additional supporting information can be found online in the Supporting Information section.

Supporting File 1: cfch70016-sup-0001-SupMat.docx.